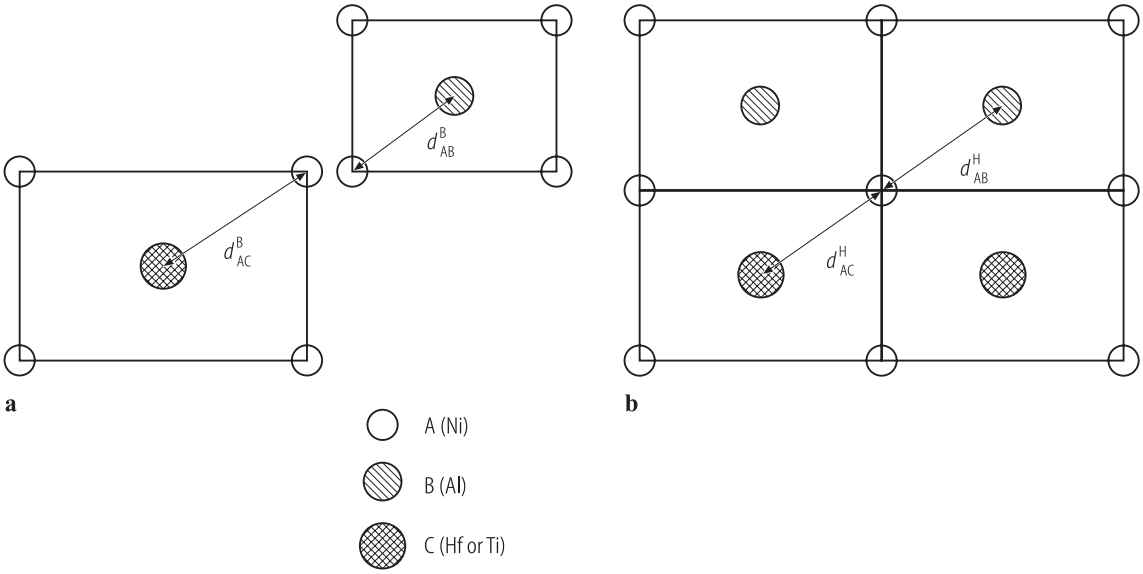

Fig. 25. Schematic illustration of (**a**) B2 structures, AB and AC compounds and (**b**) $L2_1$ structure, A_2BC compound viewing from {110} closed pack plane [90T3].

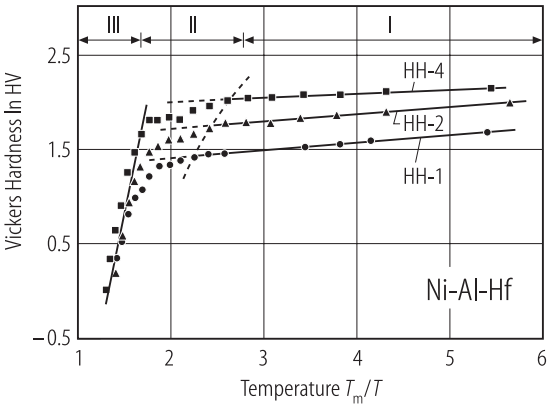

Fig. 26. Hardness HV of HH-1, HH-2 and HH-4 samples as a function of reciprocal temperature (T_m: melting point). Region (I) is the athermal process of deformation; (II) is the transition regime and region (III) is the thermally activated process of deformation [90T3].

Mg–(R)–Ag

Ternary intermetallic phases of several systems where R = La, Ce, Pr, Nd or Sm have been investigated by differential thermal analysis and X-ray diffraction.

Table 6. A summary of some physical properties of Mg–Ag–La, Mg–Ag–Ce and Mg–Ag–Pr alloys [88B1]. T_u: transformation temperature, T_a: annealing temperature (p indicates that the sample for annealing was a fine powder.), t_a: annealing time, a: lattice constant, ρ_{exp} and ρ_{calc}: mass densities, determined pyknometrically and by X-ray diffraction, respectively. Line intensity is characterized by w: weak, vw: very weak, m: medium, diff: diffuse.

Alloy	T_{liq} [°C]	T_{sol} [°C]	T_u [°C]	T_a [°C]	t_a [h]	a [pm]	Intensity of impurity lines	ρ_{exp} [g cm^{-3}]	ρ_{calc} [g cm^{-3}]
								pyknometrical	X-ray
Mg_3La	798			200 p	48	749.4 ± 2	vw		
$Mg_{2.5}Ag_{0.5}La$	710		597.5	593	20	742.6 ± 2	vw	4.035 ± 12	4.113 ± 3
Mg_2AgLa	627		581.1	595	25	734.7 ± 2	vw	4.877 ± 14	4.947 ± 4
$Mg_{1.8}Ag_{1.2}La$	619		577	560	17	731.6 ± 1	w		
$Mg_{1.6}Ag_{1.4}La$	642		570.5	535	23	729.0 ± 1	vw		
$Mg_{1.5}Ag_{1.5}La$	651		569.5	565	24	727.0 ± 2	m		
$Mg_{1.2}Ag_{1.8}La$	695	662		605	24	723.5 ± 2	vw		
$MgAg_2La$	722			640	50		diff		
Mg_3Ce	796			300 p	48	744.3 ± 1	w		
$Mg_{2.9}Ag_{0.1}Ce$	779.5								
$Mg_{2.8}Ag_{0.2}Ce$	748	702	620.7	610	10	741.1 ± 1	vw	3.616 ± 25	3.749 ± 2
$Mg_{2.6}Ag_{0.4}Ce$	733		601	590	14	738.5 ± 1	vw	4.010 ± 16	4.064 ± 2
$Mg_{2.5}Ag_{0.5}Ce$	719	647	597.4	595	24	736.7 ± 1	vw	4.172 ± 11	4.233 ± 2
$Mg_{2.4}Ag_{0.6}Ce$	698		591.5	590	24	735.4 ± 1	vw	4.321 ± 9	4.395 ± 2
$Mg_{2.2}Ag_{0.8}Ce$	659		586.5	535	80	732.6 ± 1	none	4.657 ± 14	4.728 ± 2
Mg_2AgCe	637		579	550	23	729.4 ± 2	none	5.050 ± 20	5.076 ± 4
$Mg_{1.8}Ag_{1.2}Ce$	634		572	550	21	726.7 ± 1	none	5.349 ± 18	5.422 ± 2
$Mg_{1.6}Ag_{1.4}Ce$	658	624	569.5	535	23	723.5 ± 1	none	5.677 ± 15	5.788 ± 3
$Mg_{1.4}Ag_{1.6}Ce$	695	634	560.5	570	24	721.0 ± 2	vw	6.038 ± 17	6.144 ± 5
$Mg_{1.2}Ag_{1.8}Ce$	722		559.5	560	24	718.4 ± 2	none	6.399 ± 24	6.510 ± 6
$MgAg_2Ce$	733		638	640	24	716.4 ± 2	vw	6.779 ± 22	6.867 ± 6
$Mg_{0.8}Ag_{2.2}Ce$	757			530	23	734.0 ± 3	vw		
$Mg_2Ag_{0.8}Ce_{1.2}$	656		542	540	24	724.4 ± 3	m		
$Mg_2Ag_{1.2}Ce_{0.8}$	607								
Mg_3Pr	798			200 p	40	741.6 ± 1	none		

Table 6, continued.

Alloy	T_{liq} [°C]	T_{sol} [°C]	T_u [°C]	T_a [°C]	t_a [h]	a [pm]	Intensity of impurity lines	ρ_{exp} [g cm^{-3}]	ρ_{calc} [g cm^{-3}]
								pyknometrical	X-ray
$Mg_{2.5}Ag_{0.5}Pr$	717.5	652	588	596	24	731.5 ± 1	vw	4.284 ± 11	4.337 ± 2
$Mg_{2.1}Ag_{0.9}Pr$	650		574.5	565	24	725.6 ± 2	w		
Mg_2AgPr	640		577.8	550	21	726.0 ± 2	vw	5.108 ± 14	5.162 ± 5
$Mg_{1.9}Ag_{1.1}Pr$	638		566	550	24	721.4 ± 2	vw		

Table 7. A summary of some physical properties of Ng–Ag–Pr, Mg–Ag–Nd, Mg–Ag–Sm, Mg–Ag–Gd, Mg–Ag–Tb, Mg–X–Ce (X = Cu, Au, Pd) and Cd_2AgCe [88B1]. Line intensity is characterized by w: weak, vw: very weak, m: medium, st: strong. For further explanation of symbols see Table 6.

Alloy	T_{liq} [°C]	T_{sol} [°C]	T_u [°C]	T_a [°C]	t_a [h]	a [pm]	Intensity of impurity lines	ρ [g cm^{-3}]	
								pyknometrical	X-ray
$Mg_{1.8}Ag_{1.2}Pr$	653		564	560	15	719.7 ± 1	vw		
$Mg_{1.5}Ag_{1.5}Pr$	706.5	642	544.5	530	15	715.0 ± 1	vw		
$Mg_{1.2}Ag_{1.8}Pr$	762	700	549.5	540	24	712.4 ± 2	vw		
$MgAg_2Pr$	771		678.4	674	26	709.8 ± 1	none	7.051 ± 32	7.075 ± 3
Mg_3Nd	774					741.0	none		
$Mg_{2.5}Ag_{0.5}Nd$	705	640	584.5	608	24	732.7 ± 1	vw	4.344 ± 10	4.372 ± 2
Mg_2AgNd	633		563.3	545	23	722.6 ± 1	vw	5.199 ± 14	5.293 ± 3
$Mg_{1.8}Ag_{1.2}Nd$	664	637	563	560	15	718.5 ± 3	w		
$Mg_{1.5}Ag_{1.5}Nd$	715	656	546.5	530	15	714.0 ± 3	vw		
$Mg_{1.2}Ag_{1.8}Nd$	751	714	529.5	520	24	710.5 ± 1	vw		
$MgAg_2Nd$	749		673	670	28	709.8 ± 1	w	7.077 ± 25	7.137 ± 3
Mg_3Sm	709			300 p	40	736.0 ± 2	none		
$Mg_{2.5}Ag_{0.5}Sm$	644		544.5	545	24	727.9 ± 1	vw	4.467 ± 11	4.564 ± 2

Table 7, continued.

Alloy	T_{liq} [°C]	T_{sol} [°C]	T_u [°C]	T_a [°C]	t_a [h]	a [pm]	Intensity of impurity lines	ρ [g cm^{-3}]	
								pyknometrical	X-ray
Mg_2AgSm	595		534.5	520	23	719.4 ± 1	none	5.416 ± 12	5.473 ± 3
$Mg_{1.8}Ag_{1.2}Sm$	613		526.5	510	15	714.7 ± 1	vw		
$Mg_{1.5}Ag_{1.5}Sm$	682	614	524	520	24	710.5 ± 2	none		
$Mg_{1.2}Ag_{1.8}Sm$	723	666	523.5	510	24	707.0 ± 1	vw		
$MgAg_2Sm$	736		660.5	655	17	704.5 ± 2	none	7.326 ± 26	7.415 ± 6
Mg_3Gd	780					731.0			
$Mg_{2.5}Ag_{0.5}Gd$	649			520	24	727.2 ± 2	st		
Mg_2AgGd	622			500	24	715.8 ± 2	st		
Mg_3Tb						732.0			
$Mg_{2.5}Ag_{0.5}Tb$	652			420	70	716.2 ± 2	st		
$Mg_{2.5}Cu_{0.5}Ce$	710		480.5	475	24	733.2 ± 2	none		
Mg_2CuCe	621			475	25	729.0 ± 1	m		
$Mg_{2.5}Au_{0.5}Ce$	706		634	620	24	744.0 ± 3	m		
Mg_2AuCe	637			580	24				
$Mg_{2.5}Pd_{0.5}Ce$	683		572						
Cd_2AgCe	866.5			200 p	6 weeks	665.1	m		

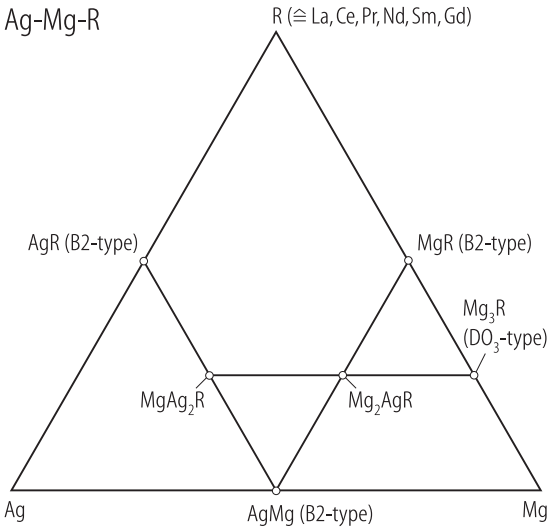

Fig. 27. Ternary phase diagram Ag–Mg–R and intermetallic compounds within the system [88B1].

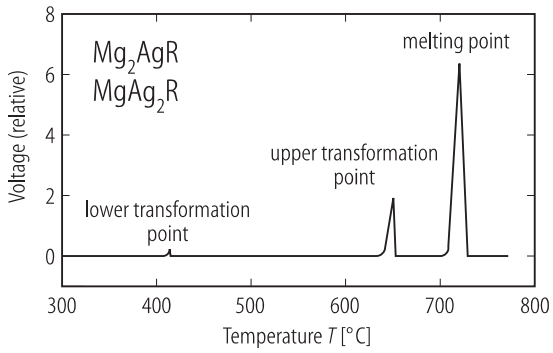

Fig. 28. Schematic diagram of the DTA recordings of phases Mg_2AgR and $MgAg_2R$ [88B1]. R: rare earth element.

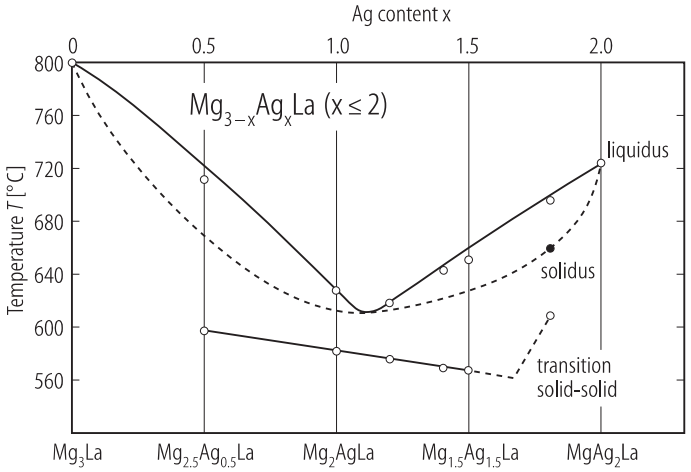

Fig. 29. Phase diagram of $Mg_{3-x}Ag_xLa$, $0 \le x \le 2$ [88B1].

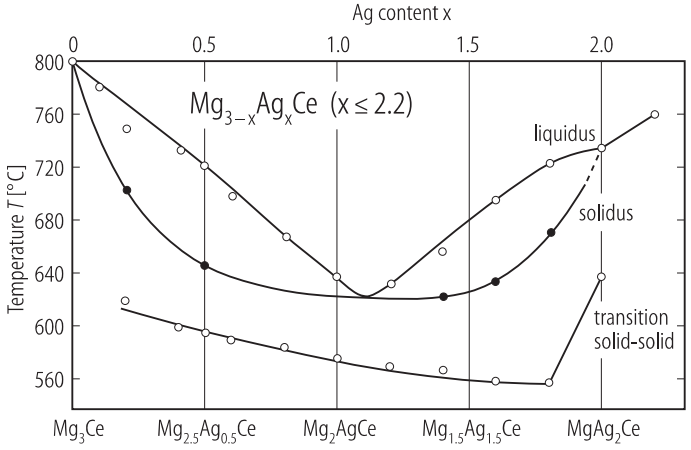

Fig. 30. Phase diagram of Mg_{3-x} Ag_xCe, $0 \le x \le 2.2$ [88B1].

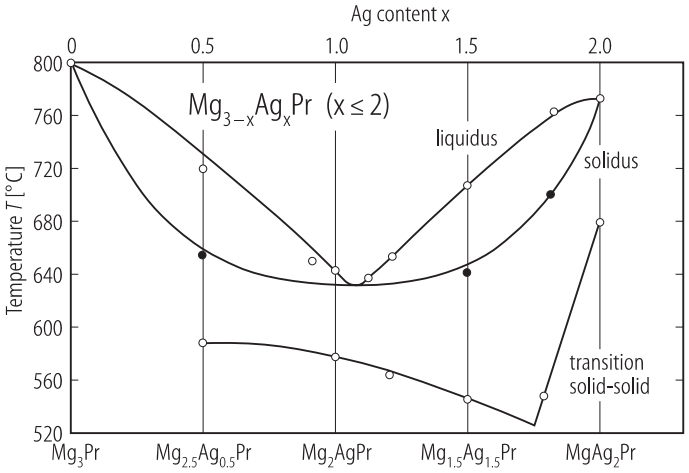

Fig. 31. Phase diagram of $Mg_{3-x}Ag_xPr$, $0 \le x \le 2$ [88B1].

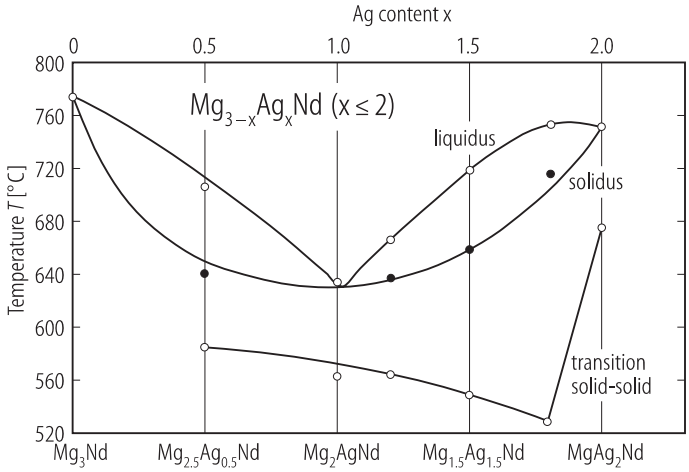

Fig. 32. Phase diagram of $Mg_{3-x}Ag_xNd$, $0 \le x \le 2$ [88B1].

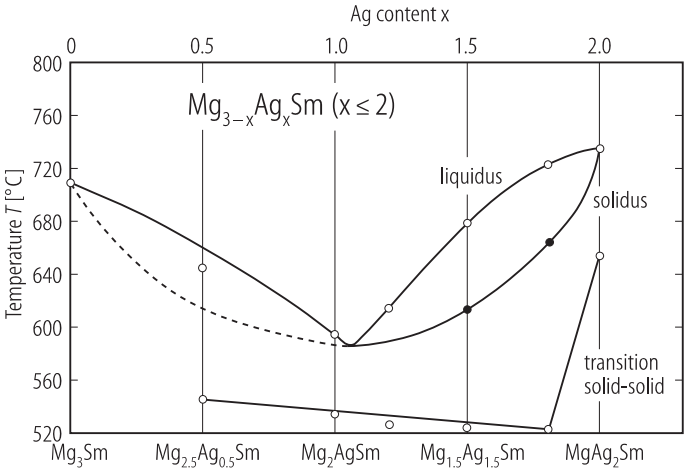

Fig. 33. Phase diagram of $Mg_{3-x}Ag_xSm$, $0 \le x \le 2$ [88B1].

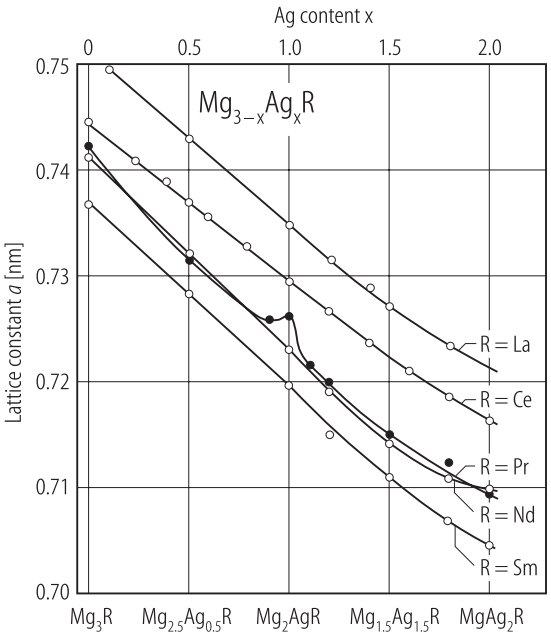

Fig. 34. Lattice constants of $Mg_{3-x}Ag_xR$ as a function of x [88B1].

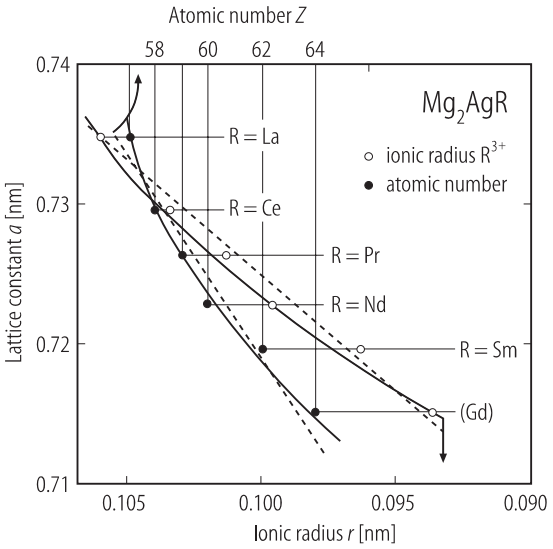

Fig. 35. Lattice constants of Mg_2AgR as a function of the atomic number Z and of the radius r (R^{3+}) respectively [88B1].

Pd–Y–Sn

The phase relations in the palladium-rich corner of the phase diagram have been extensively investigated. Five ternary phases were identified but only the Heusler β phase was found to be superconducting.

Table 8. A summary of the properties of selected alloys in the ternary phase diagram shown in Fig. 36 [85J3]. T_m: melting point, T_c: superconducting transition temperature, ρ: density.

Pd [at%]	Y [at%]	Sn [at%]	T_m [K]	Equilibrium composition at 1073 K	T_c [K]	Vickers microhardness [kgf mm^{-2}]	ρ [g cm^{-3}]
50	30	20	1413	β + Pd_5Y_4	3.65		
50	26	24		β	4	600	
50	25	25	1223	α + β	3.50		
50	25	25			5.5		
50	20	30	1233	α + β	5.20		
50	17	33	1233	α + β	5.20	560 + 575	
50	15.5	34.5	1228	α		550	9.0 ± 0.4
52	26	22	1748	β	3.75	582	8.7 ± 0.3
52	26	22			5.0		
52	24	24	1213	β + δ	5.5		
52.5	22.5	25	1213	β + ε + δ	3.2		
52.5	20	27.5	1143	β + γ + δ	4.6		
52.5	18.5	30	1153	α + β + γ	4.5		